Since January 2020 Elsevier has created a COVID-19 resource centre with free information in English and Mandarin on the novel coronavirus COVID-19. The COVID-19 resource centre is hosted on Elsevier Connect, the company's public news and information website.

Virology 539 (2020) 38–48

Contents lists available at ScienceDirect

Virology

journal homepage: www.elsevier.com/locate/virology

Porcine deltacoronavirus (PDCoV) modulates calcium influx to favor viral replication

Dongcheng Bai[a,b], Liurong Fang[a,b,*], Sijin Xia[a,b], Wenting Ke[a,b], Jing Wang[a,b], Xiaoli Wu[a,b], Puxian Fang[a,b], Shaobo Xiao[a,b]

[a] State Key Laboratory of Agricultural Microbiology, College of Veterinary Medicine, Huazhong Agricultural University, Wuhan, 430070, China
[b] Key Laboratory of Preventive Veterinary Medicine in Hubei Province, The Cooperative Innovation Center for Sustainable Pig Production, Wuhan, 430070, China

ARTICLE INFO

Keywords:
Porcine deltacoronavirus
Ca^{2+} influx
Ca^{2+} channel blocker
Viral replication

ABSTRACT

Ionic calcium (Ca^{2+}) is a versatile intracellular second messenger that plays important roles in cellular physiological and pathological processes. Porcine deltacoronavirus (PDCoV) is an emerging enteropathogenic coronavirus that causes serious vomiting and diarrhea in suckling piglets. In this study, the role of Ca^{2+} to PDCoV infection was investigated. PDCoV infection was found to upregulate intracellular Ca^{2+} concentrations of IPI-2I cells. Chelating extracellular Ca^{2+} by EGTA inhibited PDCoV replication, and this inhibitory effect was overcome by replenishment with $CaCl_2$. Treatment with Ca^{2+} channel blockers, particularly the L-type Ca^{2+} channel blocker diltiazem hydrochloride, inhibited PDCoV infection significantly. Mechanistically, diltiazem hydrochloride reduces PDCoV infection by inhibiting the replication step of the viral replication cycle. Additionally, knockdown of CACNA1S, the L-type Ca^{2+} voltage-gated channel subunit, inhibited PDCoV replication. The combined results demonstrate that PDCoV modulates calcium influx to favor its replication.

1. Introduction

The porcine deltacoronavirus (PDCoV) belongs to the newly identified genus *Deltacoronavirus* within the family *Coronaviridae* (Woo et al., 2012) and causes diarrhea, vomiting and dehydration in nursing piglets (Ma et al., 2015; Zhang, 2016). The genome of PDCoV is approximately 25.4 kb, encoding four structural proteins, three accessory proteins and 15 mature nonstructural proteins (Fang et al., 2017; Wang et al., 2019a). PDCoV was initially identified in 2012 during molecular surveillance of coronaviruses (CoVs) in mammals and birds in Hong Kong (Woo et al., 2012). In 2014, the first outbreak of PDCoV at a pig farm was reported and the virus rapidly spread to the United States (Marthaler et al., 2014; Wang et al., 2014). Subsequently, PDCoV was identified in South Korea, Canada, Mainland China, Thailand, Lao People's Democratic Republic and Vietnam (Lee and Lee, 2014; Saeng-Chuto et al., 2017; Song et al., 2015; Dong et al., 2015). Furthermore, recent studies reported that calves and chickens are also susceptible to PDCoV (Jung et al., 2017; Liang et al., 2019), and that PDCoV possesses the potential to infect humans (Li et al., 2018), highlighting a possible cross-species transmission related to this emerging virus.

Ionic calcium (Ca^{2+}) is a versatile intracellular signaling molecule that widely modulates signal transmission in cells. Ca^{2+} is involved in the regulation of a variety of processes including heart contraction, fertilization, embryonic maturation, learning, memory, cell energy metabolism, proliferation and apoptosis (Berridge et al., 2003). Ca^{2+} is maintained in the intracellular and extracellular milieu with the existence of a concentration gradient. This concentration gradient is modulated according to the demands of cells, and is controlled on the cooperation of a series of channels, transporters and pumps (Clapham, 1995). The transmembrane calcium channels include VGCC (voltage-gated calcium channels), TRP (transient receptor potential) and the CRAC channel (Ca^{2+} release and activated channel) in cell membranes, the RyR (Ryanodine receptor) and IP3R (inositol-1, 4, 5-triphosphate receptor) in the endoplasmic reticulum (ER), and the MUC (mitochondrial calcium uniporter) in the mitochondria (De Stefani et al., 2016; Gaspers et al., 2014; Hogan and Rao, 2015). Cell growth and proliferation are strictly controlled by Ca^{2+} influx with various calcium channels (Capiod, 2011). Many Ca^{2+} channel blockers that interfere with the influx of Ca^{2+} have been developed (Ehrlich et al., 1994), providing powerful tools for the study of Ca^{2+} in the pathology and progression of diseases. For example, the L-type Ca^{2+} channels, a type of VGCC, share a common pharmacological profile with high sensitivity

* Corresponding author. Laboratory of Animal Virology, College of Veterinary Medicine, Huazhong Agricultural University, 1 Shi-zi-shan Street, Wuhan, 430070, Hubei, PR China.
E-mail address: fanglr@mail.hzau.edu.cn (L. Fang).

https://doi.org/10.1016/j.virol.2019.10.011
Received 8 August 2019; Received in revised form 18 October 2019; Accepted 21 October 2019
Available online 22 October 2019

toward three classes of Ca^{2+} channel blockers, phenylalkylamines, benzothiazepines and dihydropyridines. Diltiazem, the popular heart disease drug, is a prototype of benzothiazepine that exhibits modest selectivity toward L-type Ca^{2+} channels and is currently used in the clinic (Hockerman et al., 1997; Kraus et al., 1998).

Because Ca^{2+} signaling regulates a broad range of cellular processes, it is not surprising that many viruses modulate Ca^{2+} signaling to favor their replication. For example, the Dengue virus (DENV) and West Nile virus (WNV) disturb Ca^{2+} homeostasis to favor the viral replication cycle, and cells treated with Ca^{2+} chelators and channel blockers significantly suppress the production of viral yields (Dionicio et al., 2018; Scherbik and Brinton, 2010). Rotavirus (RV) infection activates the ER calcium sensor stromal interaction molecule 1 (STIM1) and store-operated calcium entry (SOCE) to promote viral replication (Hyser et al., 2013). Hepatitis C virus (HCV) infection triggers ER Ca^{2+} depletion and increases Ca^{2+} uptake by mitochondria to induce apoptosis and mitochondrial dysfunction (Benali-Furet et al., 2005; Brault et al., 2013). In addition, studies reported that Ca^{2+} plays an important role in pore expansion and syncytium formation following virus-mediated cell-cell fusion (Ciechonska et al., 2014).

As an emerging virus, the role of Ca^{2+} in PDCoV infection remains unknown. In this study, we sought to investigate the relationship between Ca^{2+} influx and PDCoV infection. The results showed that PDCoV infection increased the intracellular Ca^{2+} levels. Treatment with Ca^{2+} chelators and channel blockers significantly decreased viral yield. We also demonstrated that the L-type Ca^{2+} channel blocker diltiazem hydrochloride decreased PDCoV infection significantly by inhibiting the replication step of the viral replication cycle.

2. Results

2.1. PDCoV infection increases the cytosolic Ca^{2+} concentration

To investigate whether PDCoV infection alters the cytosolic Ca^{2+} levels, a fluorescence-based flux assay was used to evaluate calcium levels in cells after PDCoV infection. IPI-2I cells, the porcine ileum epithelial cells that are highly susceptible to PDCoV (Wang et al., 2019b), were preloaded with the fluo-3-pentaacetoxymethyl ester (Fluo-3AM), a regent that can freely diffuse into cells and combine with free cytosolic Ca^{2+} to produce fluorescence. The preloaded cells were infected with PDCoV at a multiplicity of infection (MOI) of 3 and the fluorescence was measured at 5-min intervals. As shown in Fig. 1A, the cytosolic Ca^{2+} concentration increased after 120 min (2 h) postinfection when compared with mock-infected cells. We also measured the cytosolic Ca^{2+} changes at 5-min intervals in LLC-PK1 cells (pig kidney cells), another cell line which is also highly susceptible to PDCoV, and found that the cytosolic Ca^{2+} levels significantly increased after 80 min after PDCoV infection (Fig. 1B). In order to explore intracellular Ca^{2+} levels during entire infection cycle of PDCoV, the fluorescence was measured from 2 h postinfection (hpi) to 12 hpi in IPI-2I cells. The results showed that cytosolic Ca^{2+} levels progressively increased after PDCoV infection (Fig. 1C). Furthermore, the cells infected with PDCoV in Ca^{2+} free medium also showed a rise in the cytosolic Ca^{2+} concentration, which may be due to the release of Ca^{2+} from the ER.

2.2. Chelating extracellular Ca^{2+} by EGTA inhibits PDCoV infection

Ethylene glycol-bis (2-aminoethylether)-N, N, N′, N′-tetraacetic acid (EGTA) is a well-known extracellular Ca^{2+} chelator. First, the cytotoxicity of EGTA was tested by 3-(4, 5-Dimethylthiazol-2-yl)-2, 5-diphenyltetrazolium bromide (MTT) assay and the results showed that no obvious cytotoxicity was observed in IPI-2I cells treated with EGTA at concentrations below 2 mM (Fig. 2A). To evaluate whether the levels of extracellular Ca^{2+} concentration affect PDCoV infection, IPI-2I cells were pretreated with EGTA (0.5, 1.0, 2.0 mM) for 1 h, and then mock-infected or infected with PDCoV (MOI = 0.5). The unabsorbed viruses were removed and then cells were inoculated with medium with or without EGTA for an additional 6 h or 12 h. The cells were collected to detect the genomic mRNA of PDCoV and the expression of the viral nucleocapsid (N) protein. As shown in Fig. 2B, the amount of genomic PDCoV RNA decreased significantly in the presence of EGTA in time- and dose-dependent manners (Fig. 2B). Western blots further confirmed that treatment with EGTA downregulated the expression of the PDCoV N protein (Fig. 2B). We also determined the viral titers by the plaque assay and the results showed that EGTA treatment decreased the PDCoV yield significantly at both 6 hpi and 12 hpi (Fig. 2C). To further confirm the role of extracellular Ca^{2+} in viral replication, we also compared the growth curve of PDCoV in normal medium and calcium-free medium. The results showed that the virus titers of PDCoV in calcium-free medium were significantly lower than those in normal medium (Fig. 2D). Taken together, extracellular Ca^{2+} plays an important role in PDCoV infection.

2.3. Replenishing extracellular Ca^{2+} recovers EGTA-mediated inhibition of PDCoV yields

Because the extracellular Ca^{2+} chelator decreased PDCoV production significantly, we further tested whether replenishment of extracellular Ca^{2+} can recover virus yield. IPI-2I cell were treated with EGTA (2 mM) and then calcium chloride ($CaCl_2$) (1.0 or 2.0 mM) was added, and this was followed by infection with PDCoV (MOI = 0.5). The cells were collected at 6 and 12 hpi to determine viral RNA and protein expression, and measure viral titers. Consistent with the results shown in Fig. 2, treatment with EGTA decreased the expression of viral mRNA and N protein significantly, as well as reduce viral titers; however, the inhibitory effects were restored after the addition of $CaCl_2$ and a clear dose-dependent pattern was observed (Fig. 3A and B). These results indicate that the extracellular Ca^{2+} concentration is associated with PDCoV infection.

2.4. Intracellular Ca^{2+} chelator and channel blockers inhibit PDCoV production

To further investigate the roles of intracellular Ca^{2+} channels to PDCoV infection, Ca^{2+} channel blockers: diltiazem hydrochloride (DTZ), the L-type calcium channel blocker; bepridil hydrochloride (BP), the long-acting and non-selective calcium channel blocker; and 2-aminoethoxydiphenyl borate (2-APB), the IP3R antagonist, were used. The intracellular Ca^{2+} chelator 1, 2 bis-(2-aminophenoxy) ethane-N, N, N′, N′-tetraacetic acid acetoxymethyl ester (BAPTA-AM) was also tested. Preliminary experiments showed that no appreciable cytotoxicity to IPI-2I cells was observed at concentrations of 200 μM for DTZ, 20 μM for BP, 50 μM for 2-APB and 25 μM for BAPTA-AM as demonstrated by MTT assays. After treatment with these drugs, IPI-2I cells were infected with PDCoV (MOI = 0.5). As shown in Fig. 4, all tested drugs inhibited the expression of PDCoV mRNA and N protein significantly (Fig. 4A), as well as cause a reduction in viral titers (Fig. 4B) at 6 hpi and 12 hpi. Among the four drugs, the inhibitory effects of DTZ were the most pronounced. Thus, we chose DTZ for subsequent experiments.

2.5. Diltiazem hydrochloride (DTZ) inhibits the replication step of PDCoV infection

To further define the inhibitory effects of DTZ on PDCoV infection, IPI-2I cells were pretreated with DTZ at different concentrations (25, 50, 100 and 200 μM) and then infected with PDCoV (MOI = 0.5). The results showed that DTZ inhibited PDCoV mRNA and protein expression significantly in both dose- and time-dependent manners (Fig. 5A), and DTZ treatment also resulted in a notably significant reduction of the PDCoV titer in a dose-dependent manner at all tested time points (6, 9, 12, 15 hpi) (Fig. 5B).

To further explore the possible mechanism by which DTZ inhibits

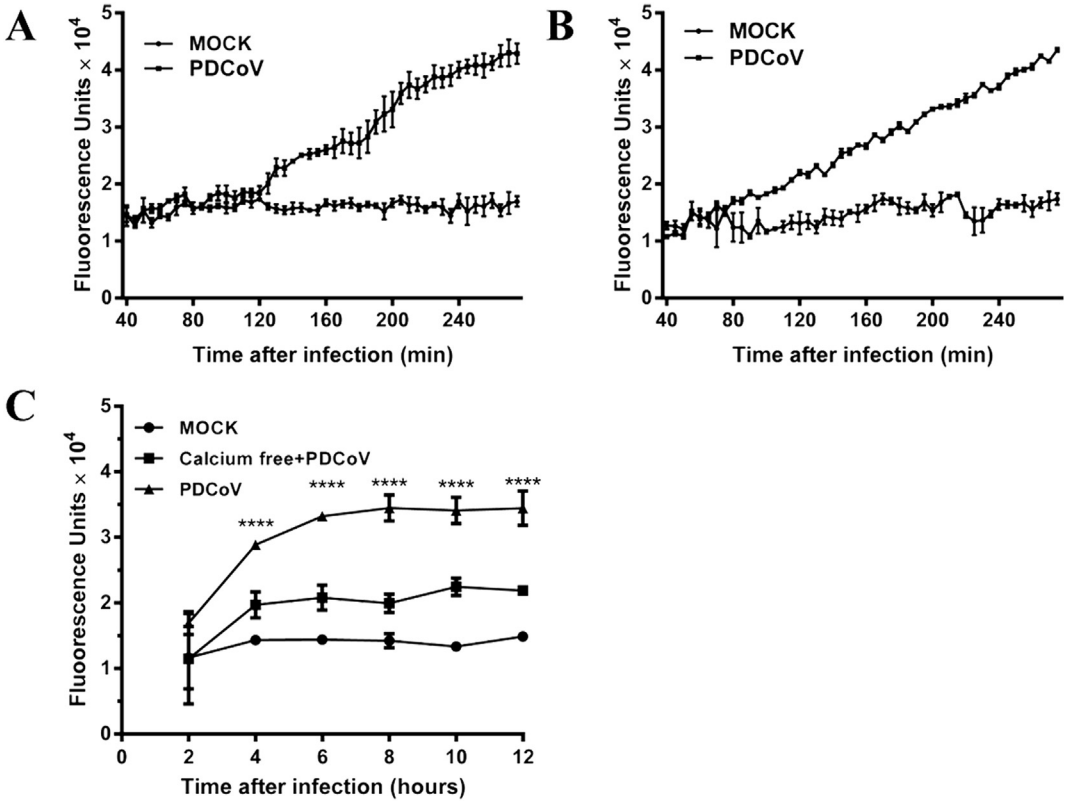

Fig. 1. Intracellular Ca^{2+} concentration during PDCoV infection. (A, B) IPI-2I cell (A) and LLC-PK1 cells (B) were preloaded with Fluo-3AM and infected with PDCoV (MOI = 3). The fluorescent absorbance values of cells were detected at 5-min intervals with a fluorescent microplate reader. (C) The cytosolic Ca^{2+} levels of IPI-2I cells were evaluated at 2-h intervals after PDCoV infection, and the cells infected with PDCoV in Ca^{2+} free medium were used as controls.

PDCoV infection, we first tested whether DTZ has an effect on direct inactivation of PDCoV particles. PDCoV was incubated with DTZ (200 μM) at 37 °C for 2 h and the virus titer was then evaluated in LLC-PK1 cells. The results showed that DTZ treatment failed to directly inactivate PDCoV (Fig. 6A).

To determine the effect of DTZ on PDCoV adsorption, IPI-2I cells cultured in 24-well plates were pretreated with DTZ (200 μM) and then inoculated with PDCoV (10, 20, 50 MOI) at 4 °C for 2 h. After three washings, the cells were collected to determine the copies of the adsorbed viruses by real-time RT-PCR. As shown in Fig. 6B, DTZ treatment did not significantly block virus attachment to IPI-2I cells at all tested infection doses (10, 20, 50 MOI).

To further evaluate the effect of DTZ on PDCoV penetration, IPI-2I cells cultured in 24-well plates were inoculated with PDCoV (0.5, 1, 2 MOI) at 4 °C for 2 h. The virus-containing medium was replaced with fresh medium containing DTZ (200 μM) and the temperature was shifted to 37 °C to allow virus entry. Two hours later, cells were washed three times and kept for another 6 h at 37 °C in DMEM with trypsin, then cells were collected and viral titers were determined by plaque assay. As shown in Fig. 6C, DTZ treatment did not block PDCoV penetration into IPI-2I cells.

To investigate whether DTZ influences the viral replication step, IPI-2I cells were infected with PDCoV (MOI = 0.5), and at 2 hpi the cell supernatants were removed and cultured in fresh medium containing DTZ (200 μM). At 6, 7, 8, 9 hpi, the infected cells were collected and PDCoV negative-sense RNA was quantified by real-time RT-PCR with primers targeting the viral 5′ UTR. As shown in Fig. 6D, DTZ treatment inhibited viral negative-sense RNA production significantly, indicating that DTZ inhibits the replication step of PDCoV infection.

We also assessed the role of DTZ on the PDCoV release step. IPI-2I cells in 24-well plates were infected with PDCoV (MOI = 0.5). At 10 hpi, the supernatants were replaced with fresh medium containing DTZ (200 μM). At 15, 30, 45 and 60 min after medium switching, the cell supernatants were harvested and titrated by the PFU assay. As shown in Fig. 6E, no noticeable differences were observed in PDCoV titers between DTZ-treated and DMSO-treated cells. These results suggested that DTZ does not inhibit PDCoV release. Taken together, these results indicated that DTZ reduces PDCoV infection through inhibiting the viral replication step but has no effect on attachment, penetration and release steps of the viral replication cycle.

2.6. Knockdown of CACNA1S inhibits PDCoV replication

DTZ is a specific blocker of the L-type Ca^{2+} channel. DTZ is well known to interact with the transmembrane segments IIIS6 and IVS6 in the L-type Ca^{2+} voltage-gated channel subunit alpha1 (CACNA1), which includes four splice isoforms CACNA1S, CACNA1C, CACNA1D and CACNA1F (Kraus et al., 1998). Because DTZ inhibits PDCoV infection, theoretically, the L-type Ca^{2+} channel should be associated with PDCoV infection. Previous studies indicated that different CACNA1 isoforms are predominant in different tissues and cell lines (Lipscombe and Andrade, 2015). We analyzed the expression abundance of different isoforms in IPI-2I cells by real-time RT-PCR and found that the mRNA expression of CACNA1S was significantly higher than others (data not shown). Thus, we further investigated whether knockdown of CACNA1S affects PDCoV infection. To this end, a recombinant lentivirus expressing CACNA1S-specific shRNA was packaged into HEK-293T cells. The knockdown efficiency of the lentivirus-based shRNA was about 50% inhibition in IPI-2I cells, as demonstrated by Western blot analysis with an antibody against CACNA1S (Fig. 7A). At the same time, we also measured the calcium oscillation in CANCA1S knockdown cells. Because the used recombinant lentivirus to knockdown CANCA1S expresses green fluorescent protein (GFP), which may interfere with the detection of calcium by Fluo-3AM. Thus, we chose

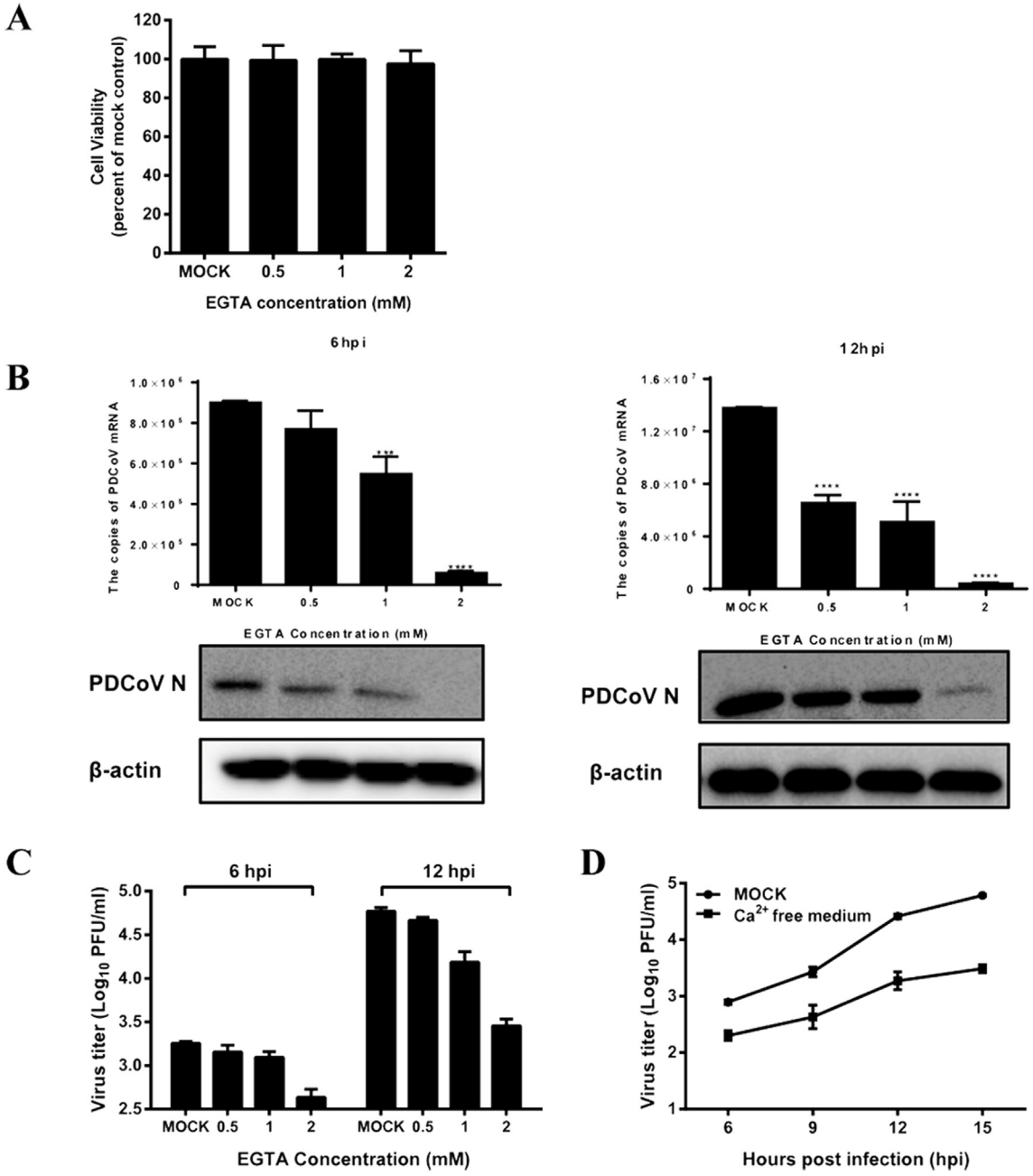

Fig. 2. EGTA treatment inhibits PDCoV production. (A) IPI-2I cells were incubated with various concentrations of EGTA or DMSO, as a control, for 12 h for the MTT assay. (B, C) IPI-2I cells were pretreated with EGTA for 1 h and then infected with PDCoV (MOI = 0.5). At 6 or 12 h post-infection (hpi), cells were collected to detect the expression of PDCoV mRNA and the N protein (B), and to measure viral titers (C). (D) IPI-2I cells were pretreated with EGTA for 1 h and then infected with PDCoV (MOI = 0.5). The infected cells were maintained with normal medium or calcium-free medium. At 6, 9 12, 15 hpi, cells were collected and viral titers were determined by plaque assay.

another calcium probe Fura-2AM to perform this experiment. As shown in Fig. 7B, the calcium oscillation induced by addition of 5 mM $CaCl_2$ was significantly lower in cells transduced with shCACNA1S compared to cells transduced shCtrl. These results indicated that knockdown of CACNA1S affects calcium oscillation. Then, IPI-2I cells were transduced with recombinant lentivirus shCACNA1S for 72 h and infected with PDCoV (MOI = 0.5) for 12 h. As expected, knockdown of CACNA1S inhibited the expression of viral mRNA and the N protein and a reduction in viral titers was observed (Fig. 7C) when compared with that of cells transduced with the control shRNA (shCtrl). Similar results could also be observed in LLC-PK1 cells (Fig. 7D).

3. Discussion

Ca^{2+} is a universal second messenger in cells, and Ca^{2+} signaling may also be an important event in the pathogenesis of viruses. In this study, we found that PDCoV infection induced Ca^{2+} oscillation. Chelating extracellular Ca^{2+} by EGTA and the intracellular Ca^{2+} by BAPTA-AM inhibited PDCoV infection. Furthermore, inhibiting Ca^{2+} channels also reduced viral yields. These results suggest that Ca^{2+} levels and channels are involved in PDCoV infection.

Ca^{2+} homeostasis is modulated by various Ca^{2+} permeable ion channels (Berridge et al., 2003). Thus, these channels are the potential targets for viruses to regulate Ca^{2+} oscillation. Influenza A virus (IAV) uses the voltage-dependent calcium channel to assist with viral entry

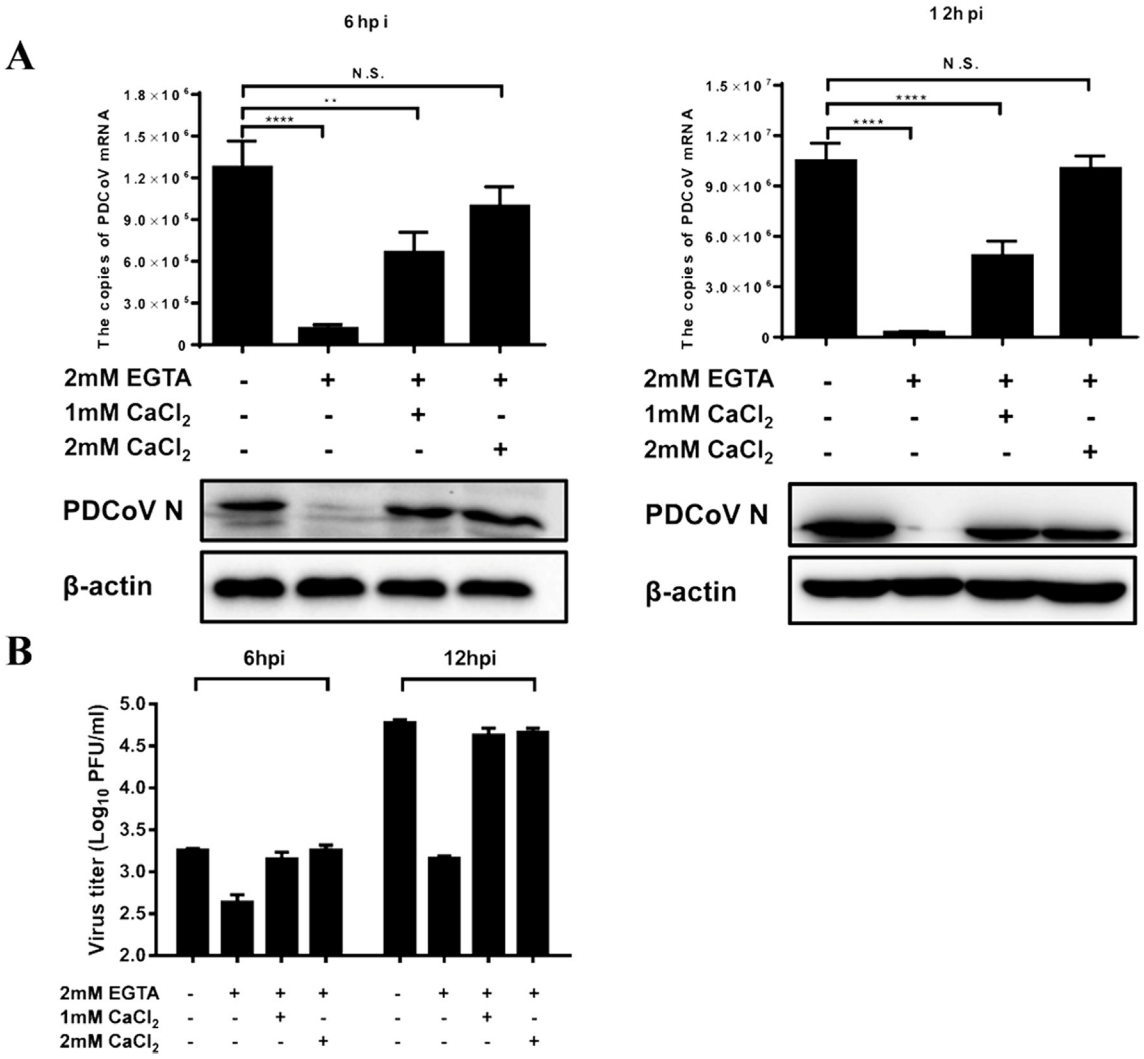

Fig. 3. Replenishing Ca^{2+} with $CaCl_2$ recovers EGTA-mediated inhibition of PDCoV infection. IPI-2I cells were treated with EGTA (2 mM) for 1 h and then $CaCl_2$ was added (1 or 2 mM). The treated cells were infected with PDCoV (MOI = 0.5). At 6 or 12 hpi, the infected cells were collected to detect the expression of PDCoV mRNA and the N protein (A), and to measure viral titers (B).

and infection (Fujioka et al., 2018). The structure of the human metapneumovirus (HPMV) M protein revealed the presence of a high-affinity Ca^{2+} binding site that promotes the stability of the protein (Leyrat et al., 2014). IAV from Aves might exist in a mineralized state with Ca^{2+}, resulting in egg-like virus-mineral structured composites, and the mineralized virus exhibits more robust infectivity and thermostability (Zhou et al., 2017). These examples suggest that Ca^{2+} and the Ca^{2+} channels are important for virus replication and are also potential antiviral targets. We tested the roles of three kinds of Ca^{2+} channel blockers that targeted the L-type calcium channel (DTZ), the long-acting and non-selective calcium channel (BP) and the IP3R channel (2-APB) to PDCoV infection. All three tested blockers reduced PDCoV yields significantly. Previous studies revealed that these blockers also exhibited inhibitory effects on the replication of the IAV, WNV, DENV and Japanese encephalitis virus (JEV) through different mechanisms (Dionicio et al., 2018; Fujioka et al., 2018; Scherbik and Brinton, 2010; Wang et al., 2017). The L-type calcium channel is a well-studied calcium channel and the main route for calcium entry into cells (Kabir et al., 2016; Robin and Allard, 2015). In this study, we found that the L-type calcium channel blocker, DTZ, exhibited a profound inhibitory effect on PDCoV infection, and DTZ mainly inhibited the viral replication stage. Apart from DTZ, the blockers BP and 2-APB also inhibited PDCoV infection significantly. Previous study showed that the blocker BP inhibits the entry of Ebola virus (EBOV) (Johansen et al., 2015). Whether the blockers BP and 2-APB target the entry or other steps in the life cycle of PDCoV infection require further studies. Recently Zhang et al. found that PDCoV infection upregulated the expression of cathepsin L and B in the endosome/lysosome to facilitate virus infection (Zhang et al., 2019). An increase in the intracellular Ca^{2+} concentration is well known to cause calpian-mediated lysosomal disruption with subsequent release of cathepsin B and L (Giorgi et al., 2008; Yamashima et al., 1998). These results are consistent with our conclusion that Ca^{2+} plays an important role in PDCoV infection.

Viruses always use their protein(s) to interact directly or indirectly with components of the Ca^{2+} signaling pathway to modulate Ca^{2+} oscillation. These viral proteins are termed as viroporins. Some viroporins have been identified, such as the non-structural protein 4 (NSP4) of rotavirus, the matrix protein 2 (M2) of IAV, the p7 protein of HCV, the viral protein U (Vpu) of HIV and the protein 2B (P2B) of picornavirus (Hyser et al., 2013; Ewart et al., 2002; Luik et al., 2009; Stouffer et al., 2008; Xie et al., 2011). These viroporins have been demonstrated to enhance the passage of ions and small molecules through membranes to favor viral replication (Nieva et al., 2012). As for CoVs, the small envelope (E) protein of the severe acute respiratory syndrome coronavirus (SARS-CoV) and Middle East respiratory syndrome coronavirus (MERS-CoV) have been demonstrated to possess ion channel

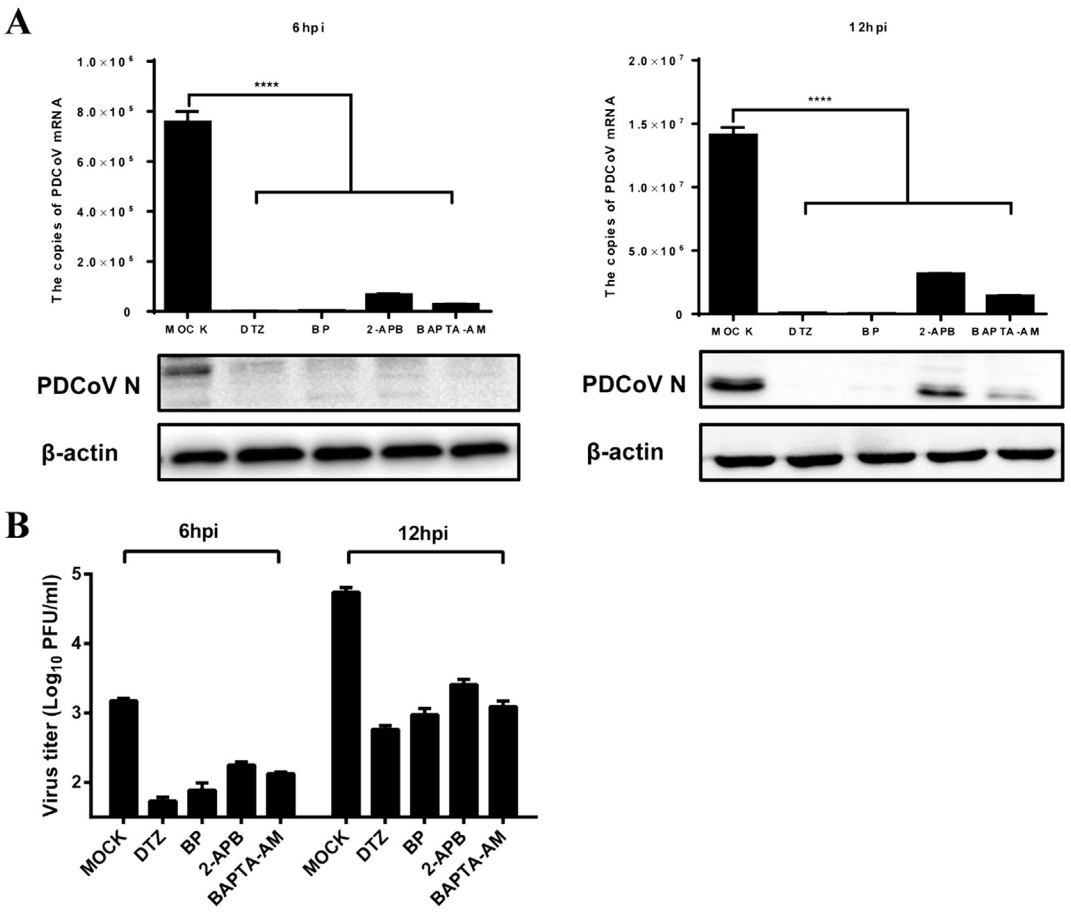

Fig. 4. Ca^{2+} channel blockers inhibit PDCoV production. IPI-2I cells were treated with diltiazem hydrochloride (DTZ, 200 μM), bepridil hydrochloride (BP, 20 μM), 2-APB (50 μM) and BAPTA-AM (25 μM) for 1 h, and then infected with PDCoV (MOI = 0.5). At 6 or 12 hpi, the infected cells were collected to detect the expression of PDCoV mRNA and the N protein (A). Viral titers were determined by the PFU assay (B).

activity (Surya et al., 2015; Verdia-Baguena et al., 2013). In addition, some accessory proteins of CoVs, such as SARS-CoV 3a and 8a, the human coronavirus 229E (HCoV-229E) 4a protein and the porcine epidemic diarrhea virus (PEDV) ORF3, have been identified as viroporins (Castano-Rodriguez et al., 2018; Wang et al., 2012; Zhang et al., 2014). PDCoV also encodes an E protein and three accessory proteins (NS6, NS7 and NS7a) (Fang et al., 2016, 2017). Our preliminary data indicated that PDCoV NS6 interacts with STIM1 (data not shown), a protein central in the regulation of SOCE (Hogan and Rao, 2015). Interestingly, STIM1 is the ER calcium sensor (Hyser et al., 2013) and PDCoV NS6 is mainly located with both the ER and the ER-Golgi during PDCoV infection (Fang et al., 2016), which make it possible to interact with STIM1 and regulate Ca^{2+} homeostasis. In addition, PDCoV NS6 is an interferon antagonist (Fang et al., 2018), and a recent study reported that STIM1 regulates the type I interferon response by retaining the signaling adaptor STING (stimulator of interferon genes) at the ER (Srikanth et al., 2019). The detailed mechanism by which NS6 regulates Ca^{2+} homeostasis and whether the interaction between PDCoV NS6 and STIM1 is involved in modulation of antiviral response and virulence are going study.

Apart from its pivotal roles in virus entry and replication, virus-induced Ca^{2+} oscillation also regulates other biological processes, such as ER stress, apoptosis and autophagy. Previous studies suggested that PDCoV infection induces apoptosis in swine testicular and LLC-PK1 cells, possibly through the activation of the cytochrome c-mediated intrinsic mitochondrial pathway (Jung et al., 2016; Lee and Lee, 2018). A recent study also showed that PDCoV infection induces autophagosome-like vesicles associated with increased autophagic activity (Qin et al., 2019). In addition, vomiting is a common clinical symptom of PDCoV-infected piglets (Zhang, 2016). Vomiting is generally induced by serotonin through activation of the enteric nervous system and extrinsic vagal afferents to the brain, whereas the release of serotonin correlates with Ca^{2+} mobilization (Jung et al., 2018). These biological processes and phenomena appear to be associated with Ca^{2+} homeostasis, and our results showed that PDCoV infection induced a Ca^{2+} oscillation. Further investigation of the relationship between the PDCoV-induced Ca^{2+} oscillation and the above-mentioned biological processes and phenomena will lead to a better understanding of the pathogenesis of PDCoV.

4. Materials and methods

4.1. Cell culture and viruses

IPI-2I, LLC-PK1 (pig kidney cells) and HEK-293T cells were cultured in Dulbecco's modified Eagle's medium (DMEM, Invitrogen) containing 10% fetal bovine serum (FBS) at 37 °C with 5% CO_2 in a humidified incubator. PDCoV strain CHN–HN-2014 (GenBank accession number: KT336560), which was isolated from a suckling piglet with severe diarrhea in China in 2014 (Dong et al., 2016), was used in this study.

4.2. Virus infection and drug treatment

The Ca^{2+} extracellular chelator EGTA (cat: 1752GR005) was purchased from BioFroxx. Diltiazem hydrochloride (cat: HY-14656), Bepridil hydrochloride (cat: HY-103315) and BAPTA-AM (cat: HY-100545) were purchased from MedChemExpress. 2-APB (cat: ab120124) was purchased from Abcam. All drugs were dissolved in

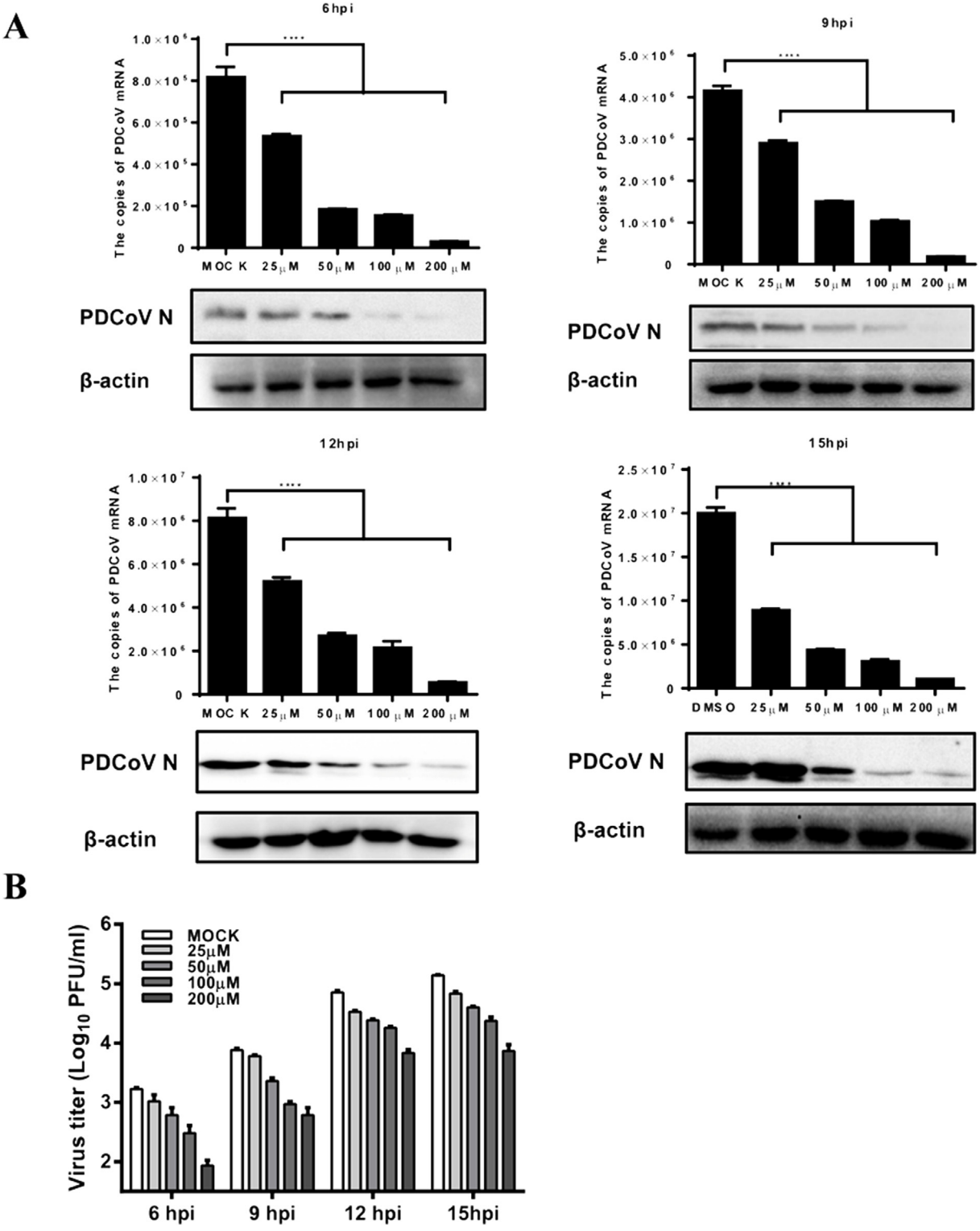

Fig. 5. Diltiazem hydrochloride inhibits PDCoV infection in a dose-dependent manner. IPI-2I cells were treated with diltiazem hydrochloride (25, 50, 100, 200 μM) and then infected with PDCoV (MOI = 0.5). At 6, 9, 12, 15 hpi, the infected cells were collected to detect the expression of PDCoV mRNA and the N protein (A). Viral titers were determined by the PFU assay (B).

DMSO or H_2O following the manufacturer's instructions. The cytotoxicity of the drugs was tested in IPI-2I cells by using an MTT assay.

For drug treatment, IPI-2I cells grown in 24-well culture plates were washed with DMEM three times, followed by the addition of fresh DMEM containing drugs for 1 h. The treated cells were then inoculated with PDCoV (MOI = 0.5) for 1 h. Subsequently, the unabsorbed viruses were removed and 1 mL of DMEM containing drugs and trypsin (2.5 μg/mL) were added. Cells were collected at the indicated time points for quantitative real-time PCR, western blotting or for virus titration analysis.

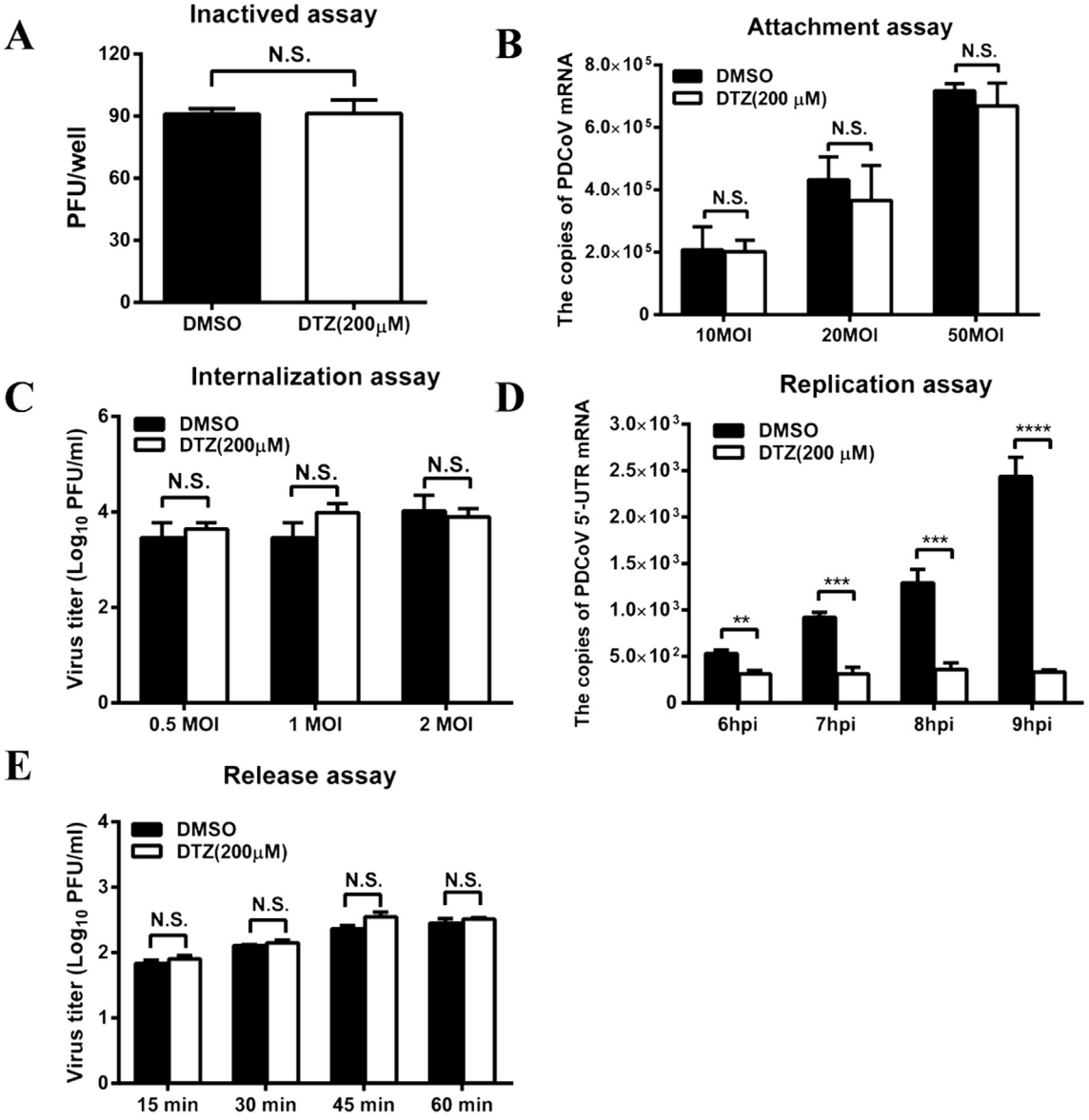

Fig. 6. Diltiazem hydrochloride inhibits the replication step of PDCoV infection. (A) Inactivated assay. PDCoV (100 PFU) was incubated with diltiazem hydrochloride (200 μM) or DMSO (dilution) at 37 °C for 2 h. The PFU assay was then performed to determine viral titers in LLC-PK1 cells. (B) Adsorption assay. IPI-2I cells cultured in 24-well plates were precooled at 4 °C for 30 min and the medium was then replaced with a mixture of diltiazem hydrochloride (200 μM) or DMSO and PDCoV (10, 20, 50 MOI). After incubation at 4 °C for another 2 h, the cells were washed with PBS and collected to detect PDCoV genomic RNA by real-time RT-PCR. (C) Penetration assay. IPI-2I cells cultured in 24-well plates were precooled at 4 °C for 30 min, and then incubated for another 2 h at 4 °C with PDCoV at different doses (0.5, 1, 2 MOI). The virus-containing medium was replaced with fresh medium containing diltiazem hydrochloride (200 μM) or DMSO, and the temperature was shifted to 37 °C for 2 h. After removing of the drug, cells were kept for another 6 h, then, collected to detect viral titers by plaque assay. (D) Replication step assay. IPI-2I cells were infected with PDCoV at a MOI of 0.5. At 2 hpi, the cell-free virus particles were removed and cells were cultured in fresh medium containing diltiazem hydrochloride (200 μM). At 6, 7, 8 and 9 hpi, the infected cells were collected for real-time RT-PCR to detect the negative-sense RNA of PDCoV. (E) Release assay. IPI-2I cells were infected with PDCoV (MOI = 0.5). At 10 hpi, the supernatants were replaced with fresh medium containing diltiazem hydrochloride (200 μM). The supernatants were harvested at 15, 30, 45 and 60 min after medium switching and titrated by the PFU assay. All results are means ± standard deviations from three independent experiments performed in triplicate.

4.3. RNA extraction and quantitative real-time PCR

Total RNA was extracted from the treated IPI-2I cells with the TRIzol reagent (Omega Bio-Tek). After the RNA was reverse-transcribed to cDNA, real-time PCR was performed to detect the genomic RNA (gRNA) and subgenomic RNA (sgRNA) of PDCoV with primers targeting the PDCoV 5′ UTR (5′ UTR-F: ACAGCACTGACTACCGTAGGGTTC, 5′ UTR-R: ATTCCACGCTCCTATGGGTATCAC) and the N gene (N–F: AGCTGCTACCTCTCCGATTC, N-R: ACATTGGCACCAGTACGAGA), respectively. Real-time PCR was performed using the SYBR green real-time PCR master mix (Applied Biosystems) in an ABI 7500 real-time PCR system (Applied Biosystems). The mRNA level of the target gene was normalized to that of glyceraldehyde-3-phosphate dehydrogenase (GAPDH) as described previously (Zhu et al., 2018).

4.4. Western blot analysis

The treated IPI-2I cells were harvested with lysis buffer (4% SDS, 3% DTT, 0.065 mM Tris-HCl [pH 6.8] and 30% glycerin) (Beyotime, China). The lysates were subjected to 10% SDS-PAGE analysis and proteins transferred to polyvinylidene difluoride membranes (Millipore, MA). The membranes were blocked with 5% skimmed milk and

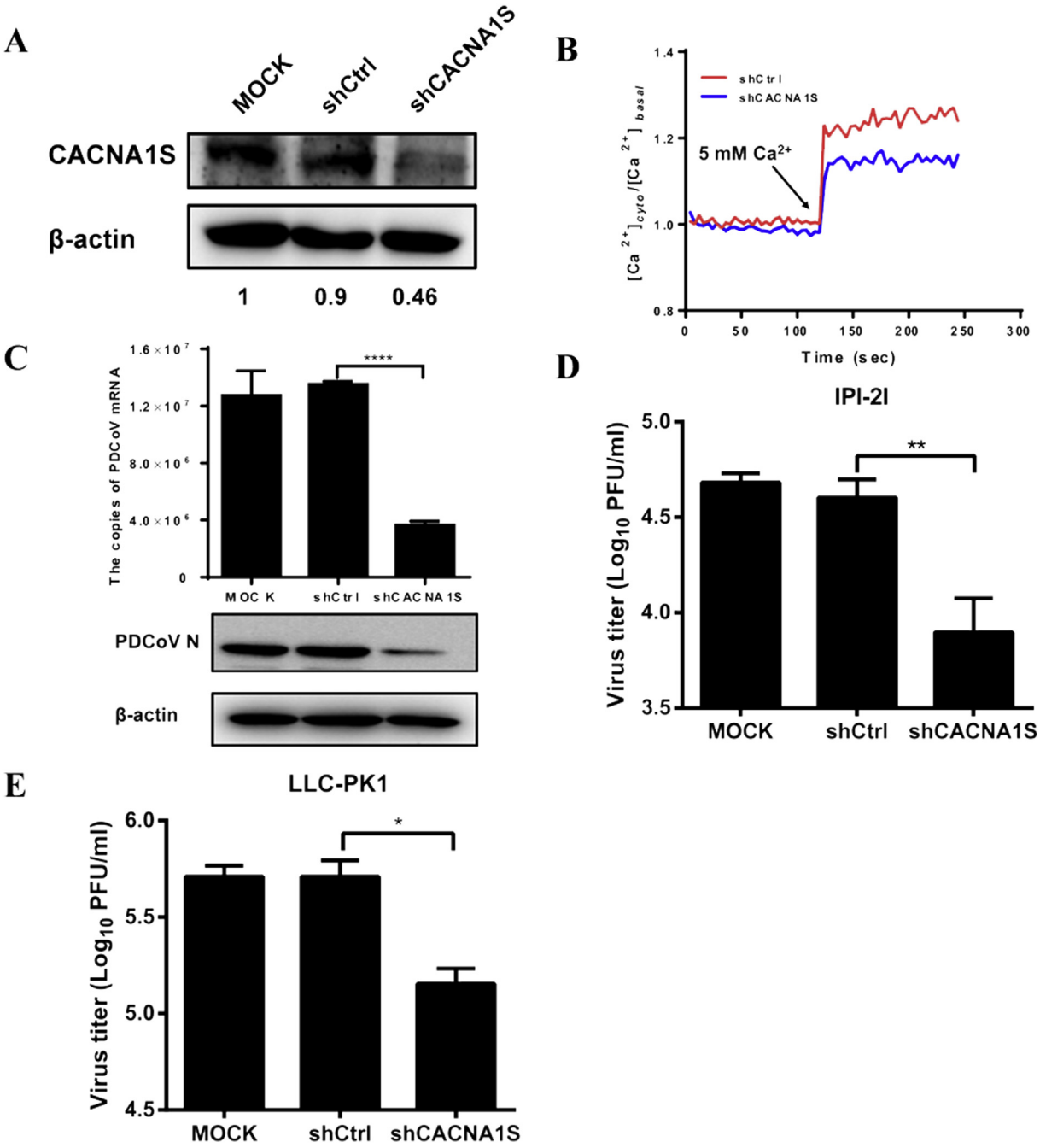

Fig. 7. Knockdown of CACNA1S inhibits PDCoV infection. (A) IPI-2I cells were transduced with recombinant lentivirus shCACNA1S or shCtrl for 72 h. The knockdown efficiency of shCACNA1S was evaluated by Western blot analysis. The relative levels of the rate of CACNA1S in comparison with the control group are shown as fold values below the images via ImageJ software analysis. (B) IPI-2I cells were transduced with recombinant lentivirus shCACNA1S or shCtrl for 72 h, and then loaded with Fura-2AM. Cytosolic Ca^{2+} oscillation was evaluated by changes in $[Ca^{2+}]_{cyto}$ induced by the addition of 5 mM $CaCl_2$. Data were normalized and expressed as $[Ca^{2+}]_{cyto}/[Ca^{2+}]_{basal}$. (C) IPI-2I cells were mock-transduced or transduced with recombinant lentivirus shCACNA1S or shCtrl for 72 h, followed by PDCoV infection (MOI = 0.5). At 12 hpi, the cells were collected to detect the expression of PDCoV mRNA and the N protein, the viral titers were determined by the plaque assay. (D) LLC-PK1 cells were transduced with lentivirus shCACNA1S or shCtrl for 72 h, and then infected with PDCoV (MOI = 0.1). At 12 hpi, cells were collected and viral titers were determine by plaque assay.

immunoblotting was carried out. An anti-PDCoV N protein monoclonal antibody was used to detect the expression of the PDCoV protein (Fang et al., 2018). An anti-CACNA1S polyclonal antibody (Bioss, bs-9925R-AP) was used to detect the expression of CACNA1S. An anti-β-actin monoclonal antibody was used to detect the expression of β-actin to confirm equal protein sample loading.

4.5. Virus titrations by the plaque assay

Virus titrations were performed using LLC-PK1 cells, as described previously (Dong et al., 2016). Briefly, LLC-PK1 cells cultured in 6-well plates were inoculated with PDCoV-containing media. After incubation at 4 °C for 2 h, the cells were washed with PBS, then covered with overlay medium (DMEM containing 0.9% (w/v) Bacto agar and 7.5 μg/mL trypsin), incubated at 37 °C for a further 24–36 h, and examined by

plaque assay. Viral titers were determined as the plaque forming unit (PFU).

4.6. Measurement of cytosolic Ca^{2+} concentrations

The intracellular Ca^{2+} concentrations were measured with Fluo-3AM (S1056, Beyotime, China). Briefly, cells seeded (5×10^4 cells/well) in 96-well plate were washed three times with Hanks' balanced salt solution (HBSS) and loaded with 100 μL of Fluo-3AM (diluted in HBSS) with 0.1% Pluronic F-127 (ST501, Beyotime) dye mix for 1 h at 37 °C. Cells were then washed with HBSS three times and cultured another 30 min at 37 °C. Cells were infected with PDCoV at an MOI of 3. Finally, the fluorescent absorbance values of cells were detected at intervals with a fluorescent microplate reader. To measure the intracellular Ca^{2+} oscillation in CANCA1S knockdown cells, IPI-2I cells were transduced with recombinant lentivirus shCACNA1S or shCtrl for 72 h, and then cells were loaded with Fura-2AM (S1052, Beyotime, diluted in HBSS) with 0.1% Pluronic F-127 (ST501, Beyotime) dye mix for 1 h at 37 °C. Cytosolic Ca^{2+} oscillation was evaluated by changes in $[Ca^{2+}]_{cyto}$ induced by the addition of 5 mM $CaCl_2$ (excitation at 340 and 380 nm, emission at 510 nm, the ratio of 340 and 380 nm fluorescence is intracellular calcium concentration). Data were normalized and expressed as $[Ca^{2+}]_{cyto}/[Ca^{2+}]_{basal}$.

4.7. shRNA and lentivirus packaging

The lentivirus knockdown plasmid pLKO.1-shCACNA1S and the control plasmid pLKO.1-shCtrl were generated by inserting the synthesized cDNA sh-CACNA1S (GGAAGTTCTTCAGCTGCAACG) and sh-Ctrl (CAACAAGATGAAGAGCACCAA) into the pLKO.1 lentivirus vector. To package the recombinant lentiviruses, HEK-293T cells were co-transfected with lentivirus-assisted plasmids pTRIP-VSV-G, pTRIP-gag-pol and pLKO.1-shCACNA1S or pLKO.1-shCtrl using Lipofectamine 2000 (Invitrogen), according to the manufacturer's instructions. The supernatants were harvested 48–72 h after co-transfection, followed by a high-speed centrifugation step (13,000 rpm) for 4 h. The pellets were suspended in serum-free DMEM and stored at −80 °C until use.

4.8. Statistical analysis

All data were analyzed with GraphPad Prism 7.0 software, using a two-tailed unpaired *t*-test. Differences between groups were considered statistically significant when the P value was less than 0.05 (*, $P < 0.05$; **, $P < 0.01$; ***, $P < 0.001$; ****, $P < 0.0001$).

Declaration of competing interest

The authors declare that there are no conflicts of interest.

Acknowledgements

This work was supported by the National Natural Science Foundation of China (31730095, U1704231, 31902247), the National Key R&D Program of China (2016YFD0500103), and the Special Project for Technology Innovation of Hubei Province (2017ABA138).

References

Benali-Furet, N.L., Chami, M., Houel, L., De Giorgi, F., Vernejoul, F., Lagorce, D., Buscail, L., Bartenschlager, R., Ichas, F., Rizzuto, R., Paterlini-Brechot, P., 2005. Hepatitis C virus core triggers apoptosis in liver cells by inducing ER stress and ER calcium depletion. Oncogene 24, 4921–4933.

Berridge, M.J., Bootman, M.D., Roderick, H.L., 2003. Calcium signalling: dynamics, homeostasis and remodelling. Nat. Rev. Mol. Cell Biol. 4, 517–529.

Brault, C., Levy, P.L., Bartosch, B., 2013. Hepatitis C virus-induced mitochondrial dysfunctions. Viruses 5, 954–980.

Capiod, T., 2011. Cell proliferation, calcium influx and calcium channels. Biochimie 93, 2075–2079.

Castano-Rodriguez, C., Honrubia, J.M., Gutierrez-Alvarez, J., DeDiego, M.L., Nieto-Torres, J.L., Jimenez-Guardeno, J.M., Regla-Nava, J.A., Fernandez-Delgado, R., Verdia-Baguena, C., Queralt-Martin, M., Kochan, G., Perlman, S., Aguilella, V.M., Sola, I., Enjuanes, L., 2018. Role of severe acute respiratory syndrome coronavirus viroporins E, 3a, and 8a in replication and pathogenesis. mBio 9, e02325-17.

Ciechonska, M., Key, T., Duncan, R., 2014. Efficient reovirus- and measles virus-mediated pore expansion during syncytium formation is dependent on annexin A1 and intracellular calcium. J. Virol. 88, 6137–6147.

Clapham, D.E., 1995. Calcium signaling. Cell 80, 259–268.

De Stefani, D., Rizzuto, R., Pozzan, T., 2016. Enjoy the trip: calcium in mitochondria back and forth. Annu. Rev. Biochem. 85, 161–192.

Dionicio, C.L., Pena, F., Constantino-Jonapa, L.A., Vazquez, C., Yocupicio-Monroy, M., Rosales, R., Zambrano, J.L., Ruiz, M.C., Del Angel, R.M., Ludert, J.E., 2018. Dengue virus induced changes in Ca^{2+} homeostasis in human hepatic cells that favor the viral replicative cycle. Virus Res. 245, 17–28.

Dong, N., Fang, L., Yang, H., Liu, H., Du, T., Fang, P., Wang, D., Chen, H., Xiao, S., 2016. Isolation, genomic characterization, and pathogenicity of a Chinese porcine deltacoronavirus strain CHN-HN-2014. Vet. Microbiol. 196, 98–106.

Dong, N., Fang, L., Zeng, S., Sun, Q., Chen, H., Xiao, S., 2015. Porcine deltacoronavirus in Mainland China. Emerg. Infect. Dis. 21, 2254–2255.

Ehrlich, B.E., Kaftan, E., Bezprozvannaya, S., Bezprozvanny, I., 1994. The pharmacology of intracellular Ca^{2+}-release channels. Trends Pharmacol. Sci. 15, 145–149.

Ewart, G.D., Mills, K., Cox, G.B., Gage, P.W., 2002. Amiloride derivatives block ion channel activity and enhancement of virus-like particle budding caused by HIV-1 protein Vpu. Eur. Biophys. J. 31, 26–35.

Fang, P., Fang, L., Hong, Y., Liu, X., Dong, N., Ma, P., Bi, J., Wang, D., Xiao, S., 2017. Discovery of a novel accessory protein NS7a encoded by porcine deltacoronavirus. J. Gen. Virol. 98, 173–178.

Fang, P., Fang, L., Liu, X., Hong, Y., Wang, Y., Dong, N., Ma, P., Bi, J., Wang, D., Xiao, S., 2016. Identification and subcellular localization of porcine deltacoronavirus accessory protein NS6. Virology 499, 170–177.

Fang, P., Fang, L., Ren, J., Hong, Y., Liu, X., Zhao, Y., Wang, D., Peng, G., Xiao, S., 2018. Porcine deltacoronavirus accessory protein NS6 antagonizes interferon beta production by interfering with the binding of RIG-I/MDA5 to double-stranded RNA. J. Virol. 92, e00712–e00718.

Fujioka, Y., Nishide, S., Ose, T., Suzuki, T., Kato, I., Fukuhara, H., Fujioka, M., Horiuchi, K., Satoh, A.O., Nepal, P., Kashiwagi, S., Wang, J., Horiguchi, M., Sato, Y., Paudel, S., Nanbo, A., Miyazaki, T., Hasegawa, H., Maenaka, K., Ohba, Y., 2018. A sialylated voltage-dependent Ca^{2+} channel binds hemagglutinin and mediates influenza a virus entry into mammalian cells. Cell Host Microbe 23, 809–818.

Gaspers, L.D., Bartlett, P.J., Politi, A., Burnett, P., Metzger, W., Johnston, J., Joseph, S.K., Hofer, T., Thomas, A.P., 2014. Hormone-induced calcium oscillations depend on cross-coupling with inositol 1,4,5-trisphosphate oscillations. Cell Rep. 9, 1209–1218.

Giorgi, C., Romagnoli, A., Pinton, P., Rizzuto, R., 2008. Ca^{2+} signaling, mitochondria and cell death. Curr. Mol. Med. 8, 119–130.

Hockerman, G.H., Peterson, B.Z., Johnson, B.D., Catterall, W.A., 1997. Molecular determinants of drug binding and action on L-type calcium channels. Annu. Rev. Pharmacol. Toxicol. 37, 361–396.

Hogan, P.G., Rao, A., 2015. Store-operated calcium entry: mechanisms and modulation. Biochem. Biophys. Res. Commun. 460, 40–49.

Hyser, J.M., Utama, B., Crawford, S.E., Broughman, J.R., Estes, M.K., 2013. Activation of the endoplasmic reticulum calcium sensor STIM1 and store-operated calcium entry by rotavirus requires NSP4 viroporin activity. J. Virol. 87, 13579–13588.

Johansen, L.M., DeWald, L.E., Shoemaker, C.J., Hoffstrom, B.G., Lear-Rooney, C.M., Stossel, A., Nelson, E., Delos, S.E., Simmons, J.A., Grenier, J.M., Pierce, L.T., Pajouhesh, H., Lehar, J., Hensley, L.E., Glass, P.J., White, J.M., Olinger, G.G., 2015. A screen of approved drugs and molecular probes identifies therapeutics with anti-Ebola virus activity. Sci. Transl. Med. 7 290ra89.

Jung, K., Hu, H., Saif, L.J., 2016. Porcine deltacoronavirus induces apoptosis in swine testicular and LLC porcine kidney cell lines in vitro but not in infected intestinal enterocytes in vivo. Vet. Microbiol. 182, 57–63.

Jung, K., Hu, H., Saif, L.J., 2017. Calves are susceptible to infection with the newly emerged porcine deltacoronavirus, but not with the swine enteric alphacoronavirus, porcine epidemic diarrhea virus. Arch. Virol. 162, 2357–2362.

Jung, K., Miyazaki, A., Saif, L.J., 2018. Immunohistochemical detection of the vomiting-inducing monoamine neurotransmitter serotonin and enterochromaffin cells in the intestines of conventional or gnotobiotic (Gn) pigs infected with porcine epidemic diarrhea virus (PEDV) and serum cytokine responses of Gn pigs to acute PEDV infection. Res. Vet. Sci. 119, 99–108.

Kabir, Z.D., Lee, A.S., Rajadhyaksha, A.M., 2016. L-type Ca^{2+} channels in mood, cognition and addiction: integrating human and rodent studies with a focus on behavioural endophenotypes. J. Physiol. 594, 5823–5837.

Kraus, R.L., Hering, S., Grabner, M., Ostler, D., Striessnig, J., 1998. Molecular mechanism of diltiazem interaction with L-type Ca^{2+} channels. J. Biol. Chem. 273, 27205–27212.

Lee, S., Lee, C., 2014. Complete genome characterization of Korean porcine deltacoronavirus strain KOR/KNU14-04/2014. Genome Announc. 2, e01191-14.

Lee, Y.J., Lee, C., 2018. Porcine deltacoronavirus induces caspase-dependent apoptosis through activation of the cytochrome c-mediated intrinsic mitochondrial pathway. Virus Res. 253, 112–123.

Leyrat, C., Renner, M., Harlos, K., Huiskonen, J.T., Grimes, J.M., 2014. Structure and self-assembly of the calcium binding matrix protein of human metapneumovirus. Structure 22, 136–148.

Li, W., Hulswit, R.J.G., Kenney, S.P., Widjaja, I., Jung, K., Alhamo, M.A., van Dieren, B., van Kuppeveld, F.J.M., Saif, L.J., Bosch, B.J., 2018. Broad receptor engagement of an emerging global coronavirus may potentiate its diverse cross-species transmissibility.

Proc. Natl. Acad. Sci. U. S. A. 115, E5135–E5143.
Liang, Q., Zhang, H., Li, B., Ding, Q., Wang, Y., Gao, W., Guo, D., Wei, Z., Hu, H., 2019. Susceptibility of chickens to porcine deltacoronavirus infection. Viruses 11, E573.
Lipscombe, D., Andrade, A., 2015. calcium channel CaValpha(1) splice isoforms - tissue specificity and drug action. Curr. Mol. Pharmacol. 8, 22–31.
Luik, P., Chew, C., Aittoniemi, J., Chang, J., Wentworth Jr., P., Dwek, R.A., Biggin, P.C., Venien-Bryan, C., Zitzmann, N., 2009. The 3-dimensional structure of a hepatitis C virus p7 ion channel by electron microscopy. Proc. Natl. Acad. Sci. U. S. A. 106, 12712–12716.
Ma, Y., Zhang, Y., Liang, X., Lou, F., Oglesbee, M., Krakowka, S., Li, J., 2015. Origin, evolution, and virulence of porcine deltacoronaviruses in the United States. mBio 6, e00064.
Marthaler, D., Raymond, L., Jiang, Y., Collins, J., Rossow, K., Rovira, A., 2014. Rapid detection, complete genome sequencing, and phylogenetic analysis of porcine deltacoronavirus. Emerg. Infect. Dis. 20, 1347–1350.
Nieva, J.L., Madan, V., Carrasco, L., 2012. Viroporins: structure and biological functions. Nat. Rev. Microbiol. 10, 563–574.
Qin, P., Du, E.Z., Luo, W.T., Yang, Y.L., Zhang, Y.Q., Wang, B., Huang, Y.W., 2019. Characteristics of the life cycle of porcine deltacoronavirus (PDCoV) in vitro: replication kinetics, cellular ultrastructure and virion morphology, and evidence of inducing autophagy. Viruses 11, E455.
Robin, G., Allard, B., 2015. Voltage-gated Ca^{2+} influx through L-type channels contributes to sarcoplasmic reticulum Ca^{2+} loading in skeletal muscle. J. Physiol. 593, 4781–4797.
Saeng-Chuto, K., Lorsirigool, A., Temeeyasen, G., Vui, D.T., Stott, C.J., Madapong, A., Tripipat, T., Wegner, M., Intrakamhaeng, M., Chongcharoen, W., Tantituvanont, A., Kaewprommal, P., Piriyapongsa, J., Nilubol, D., 2017. Different lineage of porcine deltacoronavirus in Thailand, Vietnam and Lao PDR in 2015. Transbound Emerg Dis 64, 3–10.
Scherbik, S.V., Brinton, M.A., 2010. Virus-induced Ca^{2+} influx extends survival of west nile virus-infected cells. J. Virol. 84, 8721–8731.
Song, D., Zhou, X., Peng, Q., Chen, Y., Zhang, F., Huang, T., Zhang, T., Li, A., Huang, D., Wu, Q., He, H., Tang, Y., 2015. Newly emerged porcine deltacoronavirus associated with diarrhoea in Swine in China: identification, prevalence and full-length genome sequence analysis. Transbound Emerg Dis 62, 575–580.
Srikanth, S., Woo, J.S., Wu, B., El-Sherbiny, Y.M., Leung, J., Chupradit, K., Rice, L., Seo, G.J., Calmettes, G., Ramakrishna, C., Cantin, E., An, D.S., Sun, R., Wu, T.T., Jung, J.U., Savic, S., Gwack, Y., 2019. The Ca^{2+} sensor STIM1 regulates the type I interferon response by retaining the signaling adaptor STING at the endoplasmic reticulum. Nat. Immunol. 20, 152–162.
Stouffer, A.L., Acharya, R., Salom, D., Levine, A.S., Di Costanzo, L., Soto, C.S., Tereshko, V., Nanda, V., Stayrook, S., DeGrado, W.F., 2008. Structural basis for the function and inhibition of an influenza virus proton channel. Nature 451, 596–599.
Surya, W., Li, Y., Verdia-Baguena, C., Aguilella, V.M., Torres, J., 2015. MERS coronavirus envelope protein has a single transmembrane domain that forms pentameric ion channels. Virus Res. 201, 61–66.
Verdia-Baguena, C., Nieto-Torres, J.L., Alcaraz, A., Dediego, M.L., Enjuanes, L., Aguilella, V.M., 2013. Analysis of SARS-CoV E protein ion channel activity by tuning the protein and lipid charge. Biochim. Biophys. Acta 1828, 2026–2031.
Wang, K., Lu, W., Chen, J., Xie, S., Shi, H., Hsu, H., Yu, W., Xu, K., Bian, C., Fischer, W.B., Schwarz, W., Feng, L., Sun, B., 2012. PEDV ORF3 encodes an ion channel protein and regulates virus production. FEBS Lett. 586, 384–391.
Wang, L., Byrum, B., Zhang, Y., 2014. Detection and genetic characterization of deltacoronavirus in pigs, Ohio, USA, 2014. Emerg. Infect. Dis. 20, 1227–1230.
Wang, Q., Vlasova, A.N., Kenney, S.P., Saif, L.J., 2019a. Emerging and re-emerging coronaviruses in pigs. Curr Opin Virol 34, 39–49.
Wang, S., Liu, Y., Guo, J., Wang, P., Zhang, L., Xiao, G., Wang, W., 2017. Screening of FDA-approved drugs for inhibitors of Japanese encephalitis virus infection. J. Virol. 91 e01055-17.
Wang, X., Fang, L., Liu, S., Ke, W., Wang, D., Peng, G., Xiao, S., 2019b. Susceptibility of porcine IPI-2I intestinal epithelial cells to infection with swine enteric coronaviruses. Vet. Microbiol. 233, 21–27.
Woo, P.C., Lau, S.K., Lam, C.S., Lau, C.C., Tsang, A.K., Lau, J.H., Bai, R., Teng, J.L., Tsang, C.C., Wang, M., Zheng, B.J., Chan, K.H., Yuen, K.Y., 2012. Discovery of seven novel Mammalian and avian coronaviruses in the genus deltacoronavirus supports bat coronaviruses as the gene source of alphacoronavirus and betacoronavirus and avian coronaviruses as the gene source of gammacoronavirus and deltacoronavirus. J. Virol. 86, 3995–4008.
Xie, S., Wang, K., Yu, W., Lu, W., Xu, K., Wang, J., Ye, B., Schwarz, W., Jin, Q., Sun, B., 2011. DIDS blocks a chloride-dependent current that is mediated by the 2B protein of enterovirus 71. Cell Res. 21, 1271–1275.
Yamashima, T., Kohda, Y., Tsuchiya, K., Ueno, T., Yamashita, J., Yoshioka, T., Kominami, E., 1998. Inhibition of ischaemic hippocampal neuronal death in primates with cathepsin B inhibitor CA-074: a novel strategy for neuroprotection based on 'calpain-cathepsin hypothesis. Eur. J. Neurosci. 10, 1723–1733.
Zhang, J., 2016. Porcine deltacoronavirus: overview of infection dynamics, diagnostic methods, prevalence and genetic evolution. Virus Res. 226, 71–84.
Zhang, J., Chen, J., Shi, D., Shi, H., Zhang, X., Liu, J., Cao, L., Zhu, X., Liu, Y., Wang, X., Ji, Z., Feng, L., 2019. Porcine deltacoronavirus enters cells via two pathways: a protease-mediated one at the cell surface and another facilitated by cathepsins in the endosome. J. Biol. Chem. 294, 9830–9843.
Zhang, R., Wang, K., Lv, W., Yu, W., Xie, S., Xu, K., Schwarz, W., Xiong, S., Sun, B., 2014. The ORF4a protein of human coronavirus 229E functions as a viroporin that regulates viral production. Biochim. Biophys. Acta 1838, 1088–1095.
Zhou, H., Wang, G., Wang, X., Song, Z., Tang, R., 2017. Mineralized state of the avian influenza virus in the environment. Angew Chem. Int. Ed. Engl. 56, 12908–12912.
Zhu, X., Liu, S., Wang, X., Luo, Z., Shi, Y., Wang, D., Peng, G., Chen, H., Fang, L., Xiao, S., 2018. Contribution of porcine aminopeptidase N to porcine deltacoronavirus infection. Emerg. Microb. Infect. 7, 65.